

Particle coalescing with angular momentum conservation in SPH simulations

Balázs Havasi-Tóth

Department of Hydraulic and Water Resources Engineering, Budapest University of Technology and Economics, Budapest, HUNGARY

BME-MTA Morphodynamics Research Group, Budapest, HUNGARY

Abstract

The present work introduces a simple, yet effective particle coalescing procedure for two-dimensional SPH simulations with spatially varying resolution. In addition to the regular conservation properties of former algorithms concerning the mass and linear momentum, the current model provides the exact conservation of the angular momentum as well. The detailed discussion of the coalescing method is followed by its verification through a frozen Taylor-Green vortex example with gradually derefined particle configuration. As a demonstration of the applicability of the proposed technique, a typical weakly compressible dam break simulation and an evolution of a two-dimensional Taylor-Green vortex pattern with local refinement are presented and comparisons are made with analytical and experimental data.

Keywords: smoothed particle hydrodynamics, varying resolution, particle

1. Introduction

In computational science, it is highly common during the approximate solution of partial differential equations, that some requirements significantly vary in the computational domain, such as the accuracy or the level of detail of the numerical simulation results. Thus, the application of spatially varying numerical resolution plays crucial role in cost reduction of simulations, especially in computational fluid dynamics (CFD). As it has been shown by Berger and Colella in [1], mesh-based finite volume (FVM) and even finite element methods (FEM) provide robust spatial adaptivity remarkably reducing the computational costs for simulations of several applications. Similarly, in case of particle-based Lagrangian methods adaptive resolution is also desirable, though the implementation of those models lies on slightly different assumptions.

One of the most fundamental and frequently referred meshless numerical technique is the Smoothed Particle Hydrodynamics (SPH) scheme. The first model using SPH has been constructed by Gingold and Monaghan in 1977 [2] and independently in the same year by Lucy [3]. Initially, the method

was developed for simulating astrophysical phenomena, implying large-scale self-gravitating gaseous systems in absence of boundary conditions. Later, utilizing the special properties of SPH, the method has been successfully applied for the simulation of both solid and fluid phases by Monaghan and Gray et al. [4, 5]), making SPH recently an increasingly applied theory in ocean engineering and several other fields (see [6–8]). Although the theory behind the variable smoothing lengths of the particles in SPH had been long since formulated by Gingold [9] and Monaghan [10], in order for the resolution in a specific region to be increased, particles need to be properly inserted and removed from the computational domain.

Based on different approaches, several techniques for spatially varying resolution have been introduced during the past two decades. Firstly, Kitsionas and Whitworth [11] presented a particle splitting method for astrophysical simulations while Liu [12] achieved locally increased resolution using a Delaunay triangulation. Later, Lastiwka [13] constructed criteria for local particle addition and removal with the interpolation of flow conditions and the distribution of particle mass. The precise splitting technique presented in [14] by Feldman and Bonet became one of the most widely used methods developed further by López and Roose, Vacondio et al., Liu et al., Wang et al., Xiong et

al. and Hu et al. (see [15–20]) and extended for shallow water formulations by Vacondio et al. [21, 22]. As a noteworthy idea, Barcarolo [23] and Chiron et al. [24] applied a similar splitting scheme but without the deletion of the mother particles. Instead by turning them into passive tracers, they can be implied in the flow again later, and the daughter particles can be simply deleted when leaving the high-resolution zone.

Most recently, another approach in spatially varying resolution is based on the coupling of different fluid simulations by Bouscasse et al. and Marrone et al. [25, 26] as a realization of a coupling of SPH fluid flows of different particle sizes. Such implementation is also presented by Bian et al. [27] where coupled SPH domains are overlapped through a buffer zone, in which fluid conditions are being interpolated between the zones using an overlapping interface.

According to the knowledge of the author, none of the existing particle coalescing techniques within the SPH framework provides the conservation of angular momentum. Regardless of the coarsening procedure, the aforementioned techniques reduce the degrees of freedom of the original configuration so that the angular momentum inevitably vanishes in the merged or redefined configuration. In the present work, a particle coalescing technique is

introduced, which exactly preserves not only the mass and the linear momentum, but the angular momentum as well without significant additional computational cost compared to the existing methods.

2. Motivation

The particle merging process introduced by Vacondio et al. [28] performs coalescing of particle pairs in such a way that a candidate particle a and its closest neighbor b are replaced with a new particle m in the common center of mass of particles a and b . As it has been shown in [28], pairwise coalescing process can be formulated so that mass and linear momentum are exactly preserved. However, during the merge, the degrees of freedom of the local particle set $\{a, b\}$ and $\{m\}$ is reduced from 4 to 2 in two dimensions. As a result, in case of the velocity vectors of the original pair of particles are not equal ($\mathbf{v}_a \neq \mathbf{v}_b$), the merge leads to a complete loss of angular momentum. The basic idea behind the proposed resolution reduction technique is that in two dimensions the angular momentum can be preserved only if the remaining degrees of freedom after merging is at least 4. Thus, in the present work we introduce a modified particle coalescing technique in which the particle merging is performed over particle triplets instead of pairs. The difference

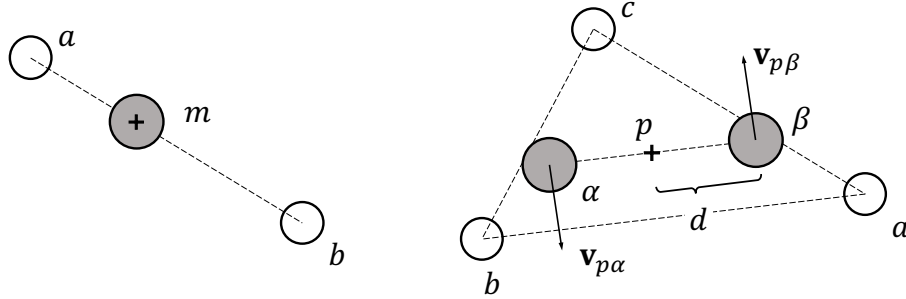


Figure 1: Coalescing of a particle pair (left) and a triplet (right). The original and the new particle layout are shown by the empty and shaded circles respectively.

between the two methods is shown in Figure 1. After merging, a triplet $\{a, b, c\}$ is replaced with a pair of identical particles $\{\alpha, \beta\}$, reducing the initial degrees of freedom from 6 to 4, which is still sufficient to preserve both the local linear and angular momenta of the original layout.

3. The merging procedure

Besides the criteria of the pre-defined refinement zones, in the present work, a particle is chosen to be a candidate for coalescing when its mass does not exceed the 90% of the mass corresponding to the original coarse resolution. Also, similarly to the process proposed by [28], the triplet is formed using the two closest neighbors of the candidate particle. To avoid a particle to be selected for two candidates in the same time step, the selection process

excludes all particles that are already marked for coalescing. The merging of the triplets is performed only after all candidates have been processed – either found neighbors or not.

3.1. Conservation of mass and linear momentum

Before placing the new particles, the position and velocity of the center of mass of the particles to be merged need to be computed. Furthermore, by keeping these quantities the same before and after the merge, the linear momentum is also preserved. As a result, we require, that:

$$\begin{aligned}\mathbf{r}_p &= \frac{\mathbf{r}_a m_a + \mathbf{r}_b m_b + \mathbf{r}_c m_c}{m_a + m_b + m_c} = \frac{\mathbf{r}_\alpha m_\alpha + \mathbf{r}_\beta m_\beta}{m_\alpha + m_\beta}, \\ \mathbf{v}_p &= \frac{\mathbf{v}_a m_a + \mathbf{v}_b m_b + \mathbf{v}_c m_c}{m_a + m_b + m_c} = \frac{\mathbf{v}_\alpha m_\alpha + \mathbf{v}_\beta m_\beta}{m_\alpha + m_\beta}.\end{aligned}\tag{1}$$

The exact conservation of mass is also enforced by choosing the new masses as

$$m_\alpha = m_\beta = m_m = \frac{m_a + m_b + m_c}{2}.\tag{2}$$

3.2. Computation of the smoothing length and the new positions

As it has been pointed out by Feldman and Bonet [14], to minimize the influence of the change in the particle layout on the solution, the minimization of the density variation during particle splitting and coalescing is of crucial importance. In attempt to minimize the change in the density field, we

compute the density at \mathbf{r}_p for both the original and coalesced layout, which therefore should be equal:

$$\langle \rho_p \rangle = \sum_{i=a,b,c} m_i W(|\mathbf{r}_p - \mathbf{r}_i|, h_i) = (m_\alpha + m_\beta) (W(|\mathbf{r}_p - \mathbf{r}_\alpha|, h_\alpha)) = (m_\alpha + m_\beta) W_{p\alpha}, \quad (3)$$

where for the sake of simplicity of the subsequent assumptions, we consider the two-dimensional Gaussian smoothing kernel function

$$W(r, h) = \frac{1}{\pi h^2} \exp\left(-\frac{r^2}{h^2}\right). \quad (4)$$

In contrast with [28], the smoothing radius cannot be computed directly due to $r \neq 0$ takes place in (4). Furthermore, as it is visualized in Figure 2, normalized kernels cannot produce arbitrary high values at a given place by varying the smoothing radius, therefore the distance $d = |\mathbf{r}_\alpha - \mathbf{r}_\beta|/2$ should be chosen carefully to avoid infeasible solutions of (3). To compute the maximum distance $r_{max} = |\mathbf{r}_\alpha - \mathbf{r}_p| = |\mathbf{r}_\beta - \mathbf{r}_p|$, at which (3) can be satisfied, (4) has been analytically analysed. Firstly, using the known value of $W_{p\alpha}$ from (3), consider the inverse of the Gaussian kernel function:

$$r = h \sqrt{-\ln(W_{p\alpha} \pi h^2)}. \quad (5)$$

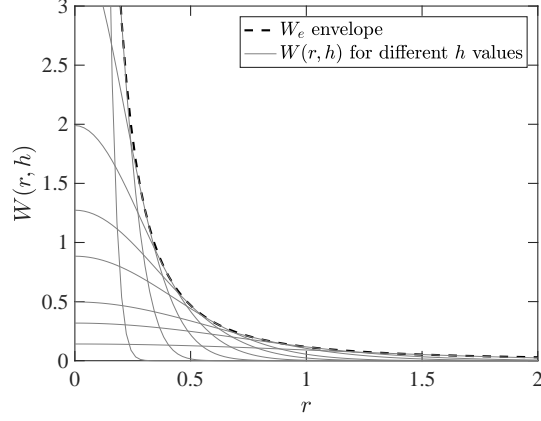


Figure 2: Gaussian kernel functions with different smoothing radii (gray solid curves) and the envelope (black dashed curve) marking the maxima of x for the corresponding values of $W(x, h)$.

To find its maxima, the derivative with respect to the smoothing length is computed and constrained to zero as follows

$$\frac{\partial r}{\partial h} = -\frac{\ln(W_{p\alpha}\pi h^2) + 1}{\sqrt{-\ln(W_{p\alpha}\pi h^2)}} = 0. \quad (6)$$

This equation has finite roots only if the numerator is zero, thus the solution of

$$\ln(W_{p\alpha}\pi h^2) = -1 \quad (7)$$

gives

$$h_{max} = \pm \sqrt{\frac{1}{e\pi W_{p\alpha}}}, \quad (8)$$

from which the positive value is the smoothing length corresponding to the maximum value of the distance r_{max} for a given value of W . Finally, substituting h_{max} to (5) gives

$$r_{max} = \sqrt{-\frac{1}{e\pi W_{p\alpha}} \ln\left(\frac{W_{p\alpha}\pi}{e\pi W_{p\alpha}}\right)} = \sqrt{\frac{1}{e\pi W_{p\alpha}}} = h_{max}, \quad (9)$$

which yields that $x = h$ is a nullcline of (5) for arbitrary W , shown in Figure 3. From (9), the envelope Figure 2 of the Gaussian kernel can be expressed as

$$W_e = \frac{1}{e\pi x^2}. \quad (10)$$

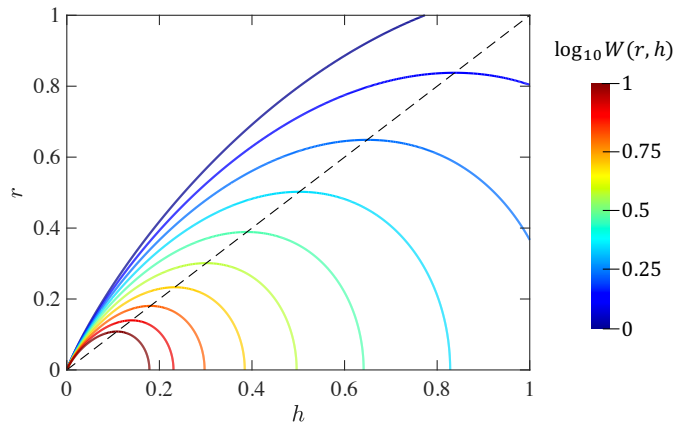


Figure 3: Isocurves of the Gaussian kernel on the $r - h$ plane (solid lines), and the $r = h$ nullcline (dashed line).

Although the maximum distance $r_{max} = |\mathbf{r}_\alpha - \mathbf{r}_p|$ can be computed from the simple expression (9), the optimal distance is usually smaller. In the

present work, the new spacing was chosen to be equal to the average distance of the original particles from \mathbf{r}_p :

$$d = \eta \frac{1}{3} \sum_{i=a,b,c} |\mathbf{r}_i - \mathbf{r}_p|, \quad (11)$$

where η is a scaling constant, which results a uniform particle distribution when set between 0.9 and 1, and d limited to r_{max} only if $d \geq r_{max}$. Otherwise the smoothing radius $h_\alpha = h_\beta$ needs to be computed. Since (4) cannot be solved directly for h , the iterative solution

$$h^{n+1} = \sqrt{\frac{1}{\pi W_{p\alpha}} \exp\left(-\frac{r^2}{(h^n)^2}\right)} \quad (12)$$

is used, where the superscript denotes the iteration level and $h^0 = h_{max}$. The iteration is terminated when the

$$10^{-6} > \left| \frac{h^{n+1} - h^n}{h^n} \right| \quad (13)$$

exiting criterion is satisfied.

After computing the distance d and smoothing radius h , the positions \mathbf{r}_α and \mathbf{r}_β are obtained using the simple constraint

$$\mathbf{r}_\alpha - \mathbf{r}_\beta \quad || \quad \max(\mathbf{r}_{ab}, \mathbf{r}_{ac}, \mathbf{r}_{bc}). \quad (14)$$

3.3. Conservation of angular momentum

The linear momentum is exactly preserved if the

$$\sum_{i=a,b,c} m_i \mathbf{v}_i = m_\alpha \mathbf{v}_\alpha + m_\beta \mathbf{v}_\beta = m_m (\mathbf{v}_\alpha + \mathbf{v}_\beta) = (m_\alpha + m_\beta) \mathbf{v}_p \quad (15)$$

condition is satisfied. Considering the center of mass instead of the origin, (15) can be written in relative coordinates, implying that the linear momentum vanishes in the co-moving frame:

$$\sum_{i=a,b,c} m_i \mathbf{v}_{pi} = m_\alpha \mathbf{v}_{p\alpha} + m_\beta \mathbf{v}_{p\beta} = m_m (\mathbf{v}_{p\alpha} + \mathbf{v}_{p\beta}) = 0, \quad (16)$$

which in turn yields to

$$\mathbf{v}_{p\alpha} = -\mathbf{v}_{p\beta}, \quad (17)$$

where $\mathbf{v}_{p\alpha} = \mathbf{v}_p - \mathbf{v}_\alpha$. Thus, compared to [28], the degrees of freedom additionally implied in our model can be utilized to carry non-zero velocities without violating the linear momentum conservation.

Similarly to (16), the angular momentum conservation can be expressed in the co-moving frame. Considering that the particle layout and merging process is being performed in two dimensions, the angular momentum becomes a scalar quantity. Using (17), the angular momentum in terms of the

local center of mass reads as

$$\sum_{i=a,b,c} m_i(\mathbf{r}_{ip} \times \mathbf{v}_{ip})\mathbf{e}_k = (m_\alpha \mathbf{r}_{\alpha p} \times \mathbf{v}_{\alpha p} + m_\beta \mathbf{r}_{\beta p} \times \mathbf{v}_{\beta p})\mathbf{e}_k = (m_\alpha + m_\beta)(\mathbf{r}_{\alpha p} \times \mathbf{v}_{\alpha p})\mathbf{e}_k, \quad (18)$$

which can be directly applied to compute the velocities $\mathbf{v}_{\alpha p}$ and $\mathbf{v}_{\beta p}$, hence the velocities in the global frame can be expressed as

$$\begin{aligned} \mathbf{v}_\alpha &= \mathbf{v}_{\alpha p} + \mathbf{v}_p, \\ \mathbf{v}_\beta &= \mathbf{v}_{\beta p} + \mathbf{v}_p, \end{aligned} \quad (19)$$

where the \mathbf{v}_p velocity of the local center of mass is already known from the unmodified configuration.

4. Fluid flow modelling with SPH

This section briefly presents the most fundamental and conventional fluid flow model of the Lagrangian particle-based SPH method applied in the present work.

4.1. Governing equations

Considering the substantial or material time-derivative of any quantity A as the sum of the local and convective terms

$$\frac{dA}{dt} = \frac{\partial A}{\partial t} + v \cdot \nabla A, \quad (20)$$

the governing equations of an arbitrary, compressible inviscid fluid can be written in the Lagrangian frame [29]:

$$\begin{aligned}\frac{d\rho}{dt} &= -\rho\nabla\mathbf{v}, \\ \frac{d\mathbf{v}}{dt} &= -\frac{1}{\rho}\nabla p + \mathbf{g} + \frac{\mathbf{f}}{\rho},\end{aligned}\tag{21}$$

where ρ , p , \mathbf{v} and \mathbf{f} are the density, pressure, velocity and the sum of the specific external forces respectively and \mathbf{g} is the gravitational acceleration vector. As proposed by Monaghan [29], the weakly compressible variant of SPH is used in the present work to control compressibility with the equation of state

$$p = c^2(\rho - \rho_0),\tag{22}$$

where c is the artificially reduced speed of sound and ρ_0 is the reference density of the fluid. The speed of sound is usually tuned to keep the maximum density variations around 1% using the following condition:

$$c = 10v_{max},\tag{23}$$

where v_{max} is the expected maximum of the velocity magnitude in the specific flow problem.

4.2. The SPH discretization

SPH is a pure Lagrangian meshless collocation method for the solution of time-dependent partial differential equations (PDEs) such as (21). The fundamental idea is that any function A can be reconstructed in the domain Ω using the generalized interpolation also known as convolution [29]

$$\langle A(\mathbf{r}) \rangle = \int_{\Omega} A(\mathbf{r} - \mathbf{r}') \delta(\mathbf{r} - \mathbf{r}') d\mathbf{r}, \quad (24)$$

which, after substituting the Dirac-function $\delta(\mathbf{r} - \mathbf{r}')$ with an appropriate mollifier $W_{ij} = W(|\mathbf{r}_i - \mathbf{r}_j|)$, can be written for finite-size nodes (particles) in discrete form as

$$\langle A(\mathbf{r}_i) \rangle = \langle A_i \rangle = \sum_j A_j W_{ij} \frac{m_j}{\rho_j}, \quad (25)$$

where m_j and ρ_j are the mass and density assigned to particle j . Among several other works, a detailed introduction of the discretization procedure is given in [30] by Violeau, as well as in the review of the SPH scheme by [29].

The expression (25) can be used for the construction of the algebraic approximation of local spatial derivatives such as gradient and divergence of any function. Thus, choosing the proper differential operators – concerning conservativity and consistency properties discussed by Sigalotti et al. [31] and Vaughan [32] – the divergence of the velocity field and the pressure

gradient can be written as

$$\begin{aligned}\langle \nabla \cdot \mathbf{v}_i \rangle &= \sum_j (\mathbf{v}_j - \mathbf{v}_i) \nabla W_{ij} \frac{m_j}{\rho_j}, \\ \langle \nabla p_i \rangle &= \rho_i \sum_j \left(\frac{p_i}{\rho_i^2} + \frac{p_j}{\rho_j^2} \right) \nabla W_{ij} m_j.\end{aligned}\tag{26}$$

Through the conventional SPH discretization process, the PDE system (21) is converted into a set of ordinary differential equations (ODE's) by substituting the spatial derivatives with the SPH algebraic representations. Thus, the conventional SPH fluid-equations read as

$$\begin{aligned}\frac{d\rho_i}{dt} &= -\rho_i \sum_j (\mathbf{v}_j - \mathbf{v}_i) \frac{m_j}{\rho_j} \nabla W_{ij}, \\ \frac{d\mathbf{v}_i}{dt} &= -\sum_j \left(\frac{p_i}{\rho_i^2} + \frac{p_j}{\rho_j^2} \right) m_j \nabla W_{ij} + \mathbf{g} + \frac{\mathbf{f}_i}{\rho_i},\end{aligned}\tag{27}$$

where the subscripts denote particle i and its neighbouring particles j and $W_{ij} = W(\mathbf{r}_i - \mathbf{r}_j, h)$ is chosen to be the fifth order polynomial Wendland smoothing kernel function [33]:

$$W(q) = \begin{cases} C_d \left(1 - \frac{q}{2}\right)^4 (2q + 1) & \text{if } q \leq 2 \\ 0 & \text{if } q > 2 \end{cases},\tag{28}$$

where $q = |\mathbf{r}_{ij}|/h$, $C_d = 7/(4\pi h^2)$ is the normalization constant in two dimensions and h is the smoothing radius. In the present work, the interparticle distance is chosen to be $dx = 2.1h$.

To facilitate numerical stability and reduce spurious oscillations in the solution, the equations (27) are usually extended by artificial diffusive terms proposed by Morris et al. [34] as well as Molteni and Colagrossi [35]. Here, the stabilization terms presented by Antuono et al. [36] are applied for both the continuity and momentum equations, hence the whole system reads as:

$$\begin{aligned}\frac{d\rho_i}{dt} &= -\rho_i \sum_j (\mathbf{v}_j - \mathbf{v}_i) \frac{m_j}{\rho_j} \nabla W_{ij} + \xi hc \sum_j \Psi_{ij} \nabla W_{ij} \frac{m_j}{\rho_j}, \\ \frac{d\mathbf{v}_i}{dt} &= -\sum_j \left(\frac{p_i}{\rho_i^2} + \frac{p_j}{\rho_j^2} \right) m_j \nabla W_{ij} + \mathbf{g} + \frac{\mathbf{f}_i}{\rho_i} + \alpha hc \rho_0 \sum_j \pi_{ij} \nabla W_{ij} \frac{m_j}{\rho_j},\end{aligned}\quad (29)$$

$$p_i = c^2(\rho_i - \rho_0),$$

where $\xi = 0.1$ and $\alpha = 0.01$ are diffusion constants and

$$\Psi_{ij} = 2(\rho_j - \rho_i) \frac{\mathbf{r}_{ji}}{|\mathbf{r}_{ji}|^2} - [\langle \nabla \rho \rangle_i^L + \langle \nabla \rho \rangle_j^L], \quad (30)$$

$$\pi_{ij} = (u_j - u_i) \frac{\mathbf{r}_{ji}}{|\mathbf{r}_{ji}|^2},$$

where $\langle \nabla \cdot \rangle^L$ is the renormalized gradient formula introduced by Randles and Libersky [37] applied here for the density to fix the violation of mass conservation caused by the kernel truncation near the free surfaces. However, in cases when the system (21) implies kinematic viscosity $\nu \Delta \mathbf{v}$ in the momentum equation, the corresponding artificial diffusive term can be changed to form the final system

$$\frac{d\mathbf{v}_i}{dt} = -\sum_j \left(\frac{p_i}{\rho_i^2} + \frac{p_j}{\rho_j^2} \right) m_j \nabla W_{ij} + \mathbf{g} + \frac{\mathbf{f}_i}{\rho_i} + 2\nu \sum_j \frac{(\mathbf{v}_i - \mathbf{v}_j) \mathbf{r}_{ij}}{|\mathbf{r}_{ij}|^2} \nabla W_{ij} \frac{m_j}{\rho_j}, \quad (31)$$

where ν denotes the strength of the viscosity.

In case of zones indicating low pressure regions in SPH flow simulations, non-physical voids may be formed in the particle distribution due to the tensile instability problem. To fill the undesired cavities in the fluid, the δ^+ -SPH method is recently proposed by Sun et al. [38] applying a modified particle shifting technique (PST) that implies the tensile instability correction introduced by Monaghan [39]. Also, particles may form unisotropic linear structures in the vicinity of flattening motion leading to a rapid decay of accuracy. This behavior is usually avoided by using the PST as well. The shifting rate of the particles is computed in every time step as

$$\begin{aligned} \mathbf{r}_i^* &= \mathbf{r}_i + \delta\mathbf{r}_i, \\ \delta\mathbf{r}_i &= -CFL \frac{v_{max}}{c} (2h)^2 \sum_j \left[1 + R \left(\frac{W_{ij}}{W(\Delta x)} \right)^n \right] \nabla W_{ij} \frac{m_j}{\rho_i + \rho_j}, \end{aligned} \quad (32)$$

where \mathbf{r}^* is the new particle position, $CFL = 1.5$ is the Courant-Friedrichs-Levy number, Δx is the average interparticle distance, $n = 4$ and $R = 0.2$.

5. Results and discussion

5.1. Frozen Taylor-Green vortex

A simple case for verification of the angular momentum conservation is the investigation of a single, high resolution vortex under gradual derefinement without the presence of physical or artificial dissipation. For the initial layout, we constructed a 209×209 grid of particles in an axis-aligned origin-centered unit square with the velocity field given by the velocity field of the Taylor-Green vortex sheet

$$\mathbf{v}_0 = \begin{bmatrix} \sin(\pi(x - 0.5))\cos(\pi(y - 0.5)) \\ -\cos(\pi(x - 0.5))\sin(\pi(y - 0.5)) \end{bmatrix}. \quad (33)$$

Without moving the Lagrangian particles in space due to their velocities, the initial layout has been gradually derefined until the number of particles reached the order of magnitude of 10, which is considered to be a coarse representation of a vortex. As Figure 4 shows, similarly to the conventional particle coalescing techniques, the uniformity of the particle layout is preserved during the derefinement process. In turn, presented in Figure 5, the merging process based on the particle triplets preserves the angular momentum exactly. In comparison with pairwise coalescing techniques, our method reduces the particle number in every derefinement step with the theoretical

maximum rate of 33.3% instead of 50%. As it is visible in Figure 5, this moderate reduction rate causes the increment of the required steps (from 20 to 30 in this specific case) until reaching the desired coarse resolution.

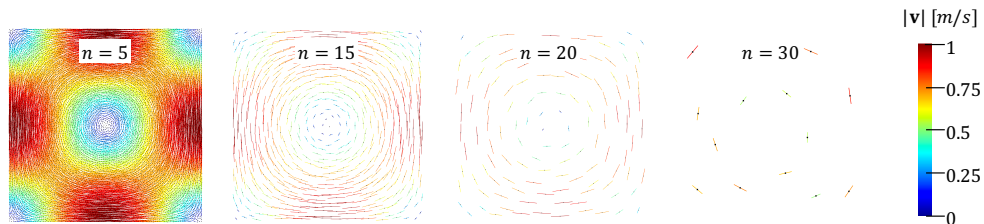


Figure 4: Particle layout during the resolution coarsening with our derefinement technique. n shows the number of derefinement steps performed from the initial grid.

5.2. Taylor-Green vortex decay

In this section, a two-dimensional Taylor-Green vortex pattern is simulated in an origin-centered periodic box with unit edge length. Similarly to the frozen Taylor-Green example in the previous section, the initial velocity field is given as

$$\mathbf{v} = v_0 \begin{bmatrix} \sin(2\pi x)\cos(2\pi y) \\ -\cos(2\pi x)\sin(2\pi y) \end{bmatrix}, \quad (34)$$

resulting in four vortices in the computational domain, where $v_0 = 1$. The simulations were performed using three different particle configurations yielding a uniformly coarse ($L/dx = 50$) and uniformly fine resolutions ($L/dx =$

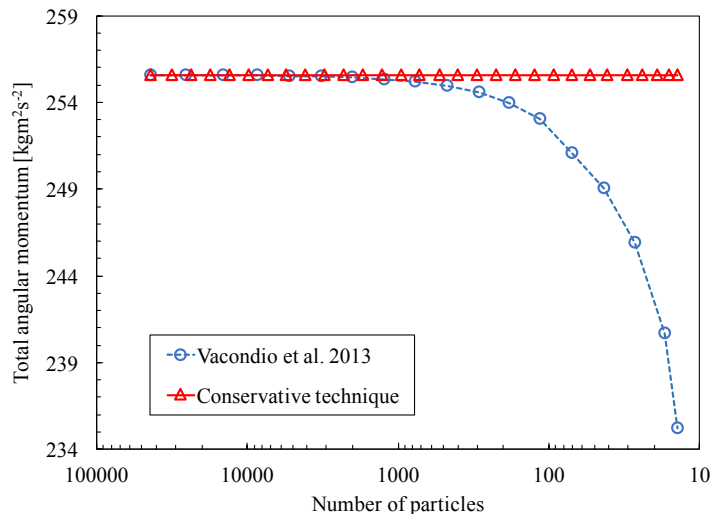


Figure 5: Total angular momentum of the vortex as a function of the number of particles while sequentially merging pairs (blue line with circles) and triplets (red line with triangles).

100) and a multi-resolution case with dynamic particle splitting and merging in a pre-defined region shown in Figure 6. The particle splitting parameters were chosen so that the refined area meet the resolution of the uniformly fine configuration. Hence, the number of daughter particles on splitting has been $n_d = 4$, $\epsilon = 0.3$, $\alpha = 0.5$, and similarly to [23], their properties concerning the mass and smoothing ratio were set to be identical. According to (34), the maximum velocity is $v_{max} = 1$ m/s, which together with the density $\rho = 1000$ kg/m³ and kinematic viscosity $\nu = 0.005$ m²/s results in $Re = v_{max}L/\nu = 200$.

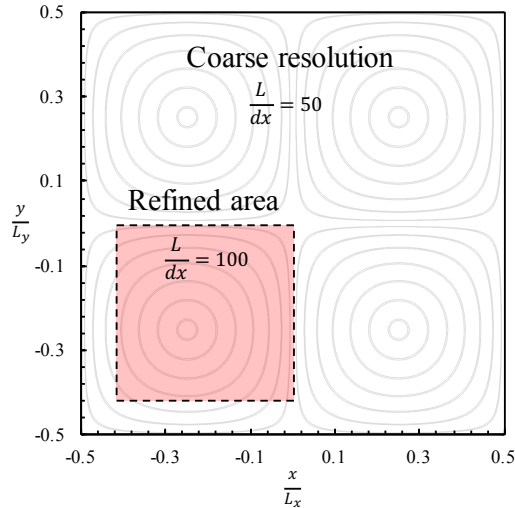


Figure 6: Two-dimensional Taylor-Green vortex pattern in periodic box using dynamic particle refinement in the marked region. Gray lines show the streamlines corresponding to the initial velocity field with the four vortices.

Due to the model of the current test case implies physical viscosity, the artificial diffusion term has been neglected in the momentum equation (29). Running the simulations to the time instant $tv_0/L = 2$ shows the results in Figure 7. Confirming that the presented coalescing technique does not affect the flow significantly, the checker-board pattern has preserved its shape in all three cases without significant distortions. To compare the accuracy of the results, the normalized total kinetic energy E/E_0 was computed for each

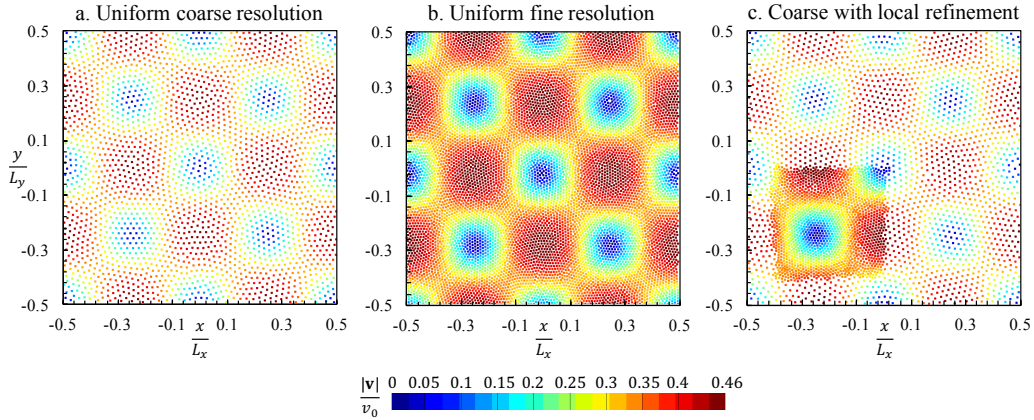


Figure 7: The simulation result of the Taylor-Green vortex decay at time instant $\frac{tv_0}{L} = 2$ using *a.* uniform coarse, *b.* locally refined, and *c.* uniform fine resolutions.

case in every instant using

$$E = \frac{1}{2} \sum_i^N m_i |\mathbf{v}_i|^2, \quad (35)$$

where m is the particle mass and E_0 is the kinetic energy of the initial flow. The kinetic energy decay is shown in Figure 8. Although the three curves present accurate evolutions compared to the analytical solution given by Krüger et al. [40], the local refinement made a significant improvement over the coarse resolution case, which together with the preserved vortex pattern verifies that no significant adverse effects had been produced by our coalescing technique in the system.

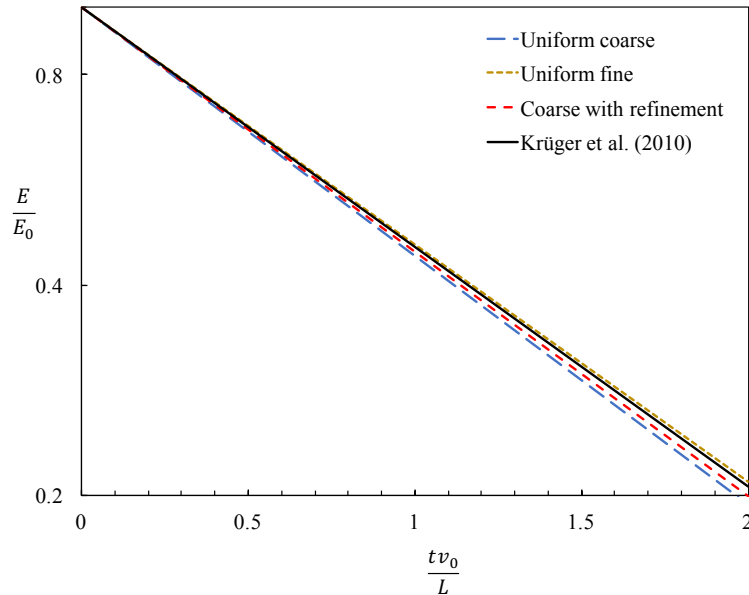


Figure 8: Total kinetic energy in case of the three different configurations.

5.3. Two-dimensional dam break

In the third test case, the applicability of the proposed method is demonstrated by a two-dimensional dam break simulation. The applied initial geometrical layout shown in Figure 9 is identical with the case experimentally investigated by Lobovský et al. [41]. Using spatially fixed fluid particles, the walls of the tank were built up as a uniform grid. For the spatially varying resolution, a rectangular region with higher desired resolution was considered in the bottom right corner. Similarly to the boundary particles, fluid particles entering this region had been split up to $n_d = 4$ refined or daughter

particles following the pattern presented in [14]. The separation parameter and smoothing ratio were set in case of both particle types to $\epsilon = 0.4$ and $\alpha = 1/\sqrt{n_d} = 0.5$ respectively. Also, during the replacement, the pattern of the small particles is rotated randomly in the fluid, but kept constant to form a uniform grid in the rigid wall. According to the merging algorithm, once a refined particle leaves and moves apart from the region farther than the initial coarse interparticle distance dx , it is marked as a candidate for coalescing and potentially merged with two of the closest particles in the neighborhood. It is important to note that new particles do not participate in further coalescing in the same time step. During the sequence of the derefinement steps, small particles gradually restore the original coarse spatial resolution. Coloring the particles according to their pressure values, six different time instants of the simulation results with the locally increased resolution are visible in Figure 10.

Besides the computation with the dynamic resolution, two further simulations were performed using uniformly coarse ($H = 81dx$) and fine resolutions ($H = 161dx$) as well. For comparison, the time series of the pressure had been evaluated at the probe p_1 on the right side of the tank marked with a yellow dot in Figure 9. To eliminate non-physical numerical oscillations, a

fixed size ($\Delta = 0.02$ s) renormalized Gaussian low-pass filter was applied on the pressure time series for each simulation result. The pressure probe time series of the three cases are shown in Figure 11.

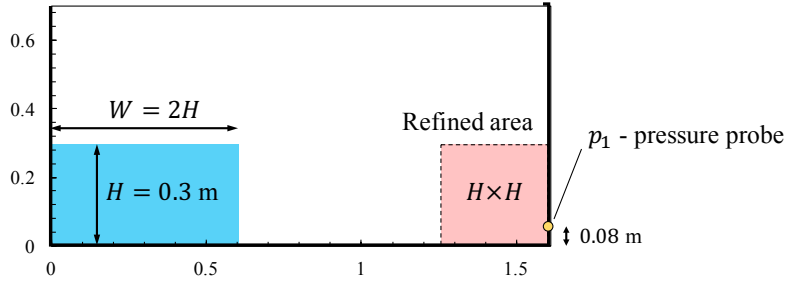


Figure 9: Initial condition of the two-dimensional dam break problem. High-resolution region is visualized with the light red rectangle in the right corner, while the yellow dot marks a pressure probe. The initial interparticle distance is denoted by dx .

6. Implementation

The proposed conservative model and the simulation cases in the present work have been implemented and run using Nauticle introduced in [42] by Tóth, the general purpose particle-based parallel simulation tool facilitating the application and development of meshless numerical methods.

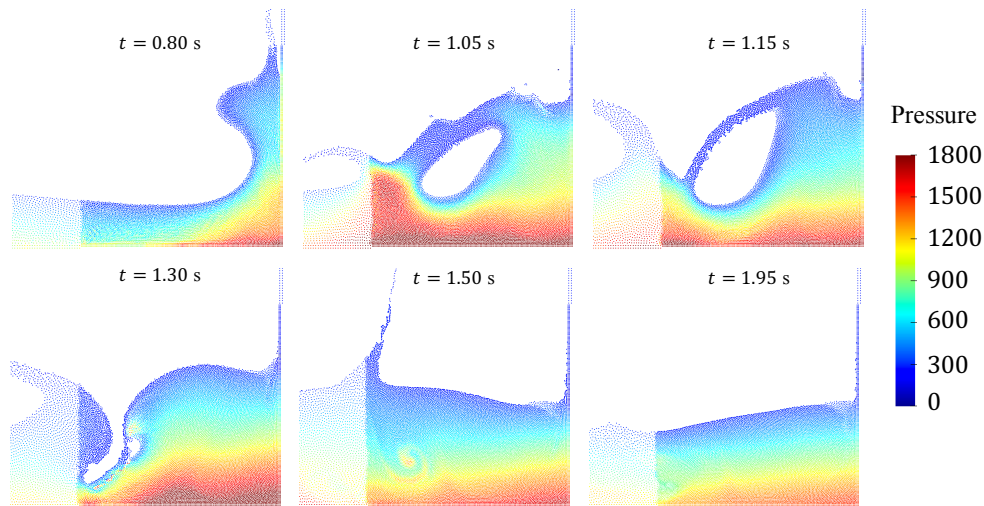


Figure 10: Different time instants of the dam break simulation with dynamic splitting and conservative merging. The figure shows the bottom right corner incorporating the zone with the local refinement.

7. Conclusion

A novel coalescing technique with exact angular momentum conservation is introduced. The method can be considered as an extension of the former pairwise merging techniques, however, some nontrivial steps are required. During the derefinement of high resolution particles, former merging techniques replace a pair of particles with a single one inevitably canceling out local rotational motion and consequently the angular momentum. In this work, to preserve angular momentum, additional degrees of freedom for the coalesced layout are achieved by replacing three particles instead of two with

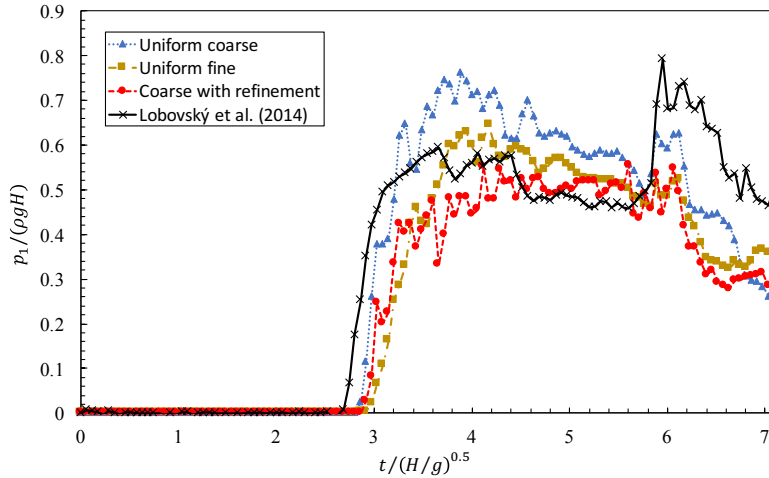


Figure 11: Dam break pressure series for different resolutions (blue solid line: uniform coarse, yellow dotted line: uniform fine, red dashed line: coarse with local refinement) evaluated at the p_1 probe. *a.* pressure time series at p_1 , *b.* Quadratic deviation of the uniform coarse and multi-resolution cases from the uniform fine resolution.

a pair of identical co-rotating particles. The smoothing radius of the coalesced particles is obtained with the inverse of the Gaussian kernel so that the density error is eliminated in the local center of mass of the particles.

The proposed method has been verified through a frozen Taylor-Green vortex example with several consecutive derefinement steps from high to low resolutions. It has been shown, that pairwise techniques suffer from significant loss of angular momentum when the resolution of the vortex becomes low. Moreover, to demonstrate the efficiency of the new particle replace-

ment scheme two-dimensional multi-resolution Taylor-Green and dam break simulations have been compared to results with uniformly coarse and fine resolutions as well as with analytical and experimental data.

Since the proposed enhancement requires only a few additional computationally cheap steps compared to pairwise methods, its application is feasible in most circumstances and provides a more accurate particle merging technique.

The extension of the introduced coalescing technique to three dimensions is also possible but probably not completely straightforward. In case of a three dimensional computation, the local particle layout has 9 and 6 degrees of freedom, before and after the coalescing respectively, which is still sufficient to preserve the angular momentum of the local configuration. Therefore there is no need to change the number of involved particles either in the initial or the merged layout. Moreover, since any three particles occupy a common plane in higher dimensions as well as in two dimensions, the presented replacement process is expected to be a proper choice. However, some difficulties might arise in cases when the local angular momentum vector is nearly parallel with the line between the merged particles. Although it is improbable for those to be exactly parallel, the conservation of the angular momentum would result

unphysically high local velocity magnitudes of the new particles.

Acknowledgement

The research reported in this paper was supported by the Higher Education Excellence Program of the Ministry of Human Capacities in the frame of Water Science & Disaster Prevention research area of Budapest University of Technology and Economics (BME FIKP-VÍZ)

References

- [1] M. Berger, C. P., Local adaptive mesh refinement for shock hydrodynamics, *Journal of computational Physics* 82 (1) (1989) 64–84.
- [2] R. Gingold, J. Monaghan, Smoothed particle hydrodynamics theory and application to non-spherical stars, *Mon. Not. R. Astron. Soc.* vol. 181 (1977) 375–389.
- [3] L. Lucy, A numerical approach to the testing of the fission hypothesis, *Astron. J.* vol. 82 (1977) 1013–1024.
- [4] J. Monaghan, Simulating free surface flows with SPH, *J. Comput. Phys.* 110 (1994) 399–406.
- [5] J. Gray, J. Monaghan, R. Swift, SPH elastic dynamics, *Comput. Methods Appl. Mech. Eng.* 190 (2001) 6641 – 6662.
- [6] S. Chowdhury, S. Sannasiraj, SPH Simulation of shallow water wave propagation, *Ocean Engineering* 60 (2013) 41–52.
- [7] R. Dalrymple, B. Rogers, Numerical modeling of water waves with the SPH method, *Coastal Engineering* 53 (2006) 141–147.

- [8] X. Sun, M. Sakai, Y. Yamada, Three-dimensional simulation of a solid-liquid flow by the DEM-SPH method, *Journal of Computational Physics* 248 (2013) 147–176.
- [9] R. Gingold, J. Monaghan, Kernel estimates as a basis for general particle methods in hydrodynamics, *Journal of Computational Physics* 46 (3) (1982) 429–453.
- [10] J. Monaghan, SPH compressible turbulence, *Monthly Notices of the Royal Astronomical Society* 335 (3) (2002) 843–852.
- [11] S. Kitsionas, A. Whitworth, Smoothed particle hydrodynamics with particle splitting, applied to self-gravitating collapse, *Monthly Notices of the Royal Astronomical Society* 330 (1) (2002) 129–136.
- [12] G.-R. Liu, *Mesh free methods: moving beyond the finite element method*, CRC press, 2002.
- [13] M. Lastiwka, N. Quinlan, M. Basa, Adaptive particle distribution for smoothed particle hydrodynamics, *International Journal for Numerical Methods in Fluids* 47 (10-11) (2005) 1403–1409.
- [14] J. Feldman, J. Bonet, Dynamic refinement and boundary contact forces

- in SPH with applications in fluid flow problems, *International Journal for Numerical Methods in Engineering* 72 (3) (2007) 295–324.
- [15] Y. López, D. Roose, Particle refinement for fluid flow simulations with SPH, *Computer Methods in Mechanics*, CMM-2011, Warsaw, Poland.
- [16] R. Vacondio, B. Rogers, P. Stansby, P. Mignosa, Variable resolution for SPH in three dimensions: Towards optimal splitting and coalescing for dynamic adaptivity, *Computer Methods in Applied Mechanics and Engineering* 300 (2016) 442–460.
- [17] W. Liu, P. Sun, F. Ming, A. Zhang, Application of particle splitting method for both hydrostatic and hydrodynamic cases in SPH, *Acta Mechanica Sinica* (2017) 1–13.
- [18] L. Wang, F. Xu, Y. Yang, J. Wang, A dynamic particle refinement strategy in smoothed particle hydrodynamics for fluid–structure interaction problems, *Engineering Analysis with Boundary Elements*.
- [19] Q. Xiong, B. Li, J. Xu, GPU-accelerated adaptive particle splitting and merging in SPH, *Computer Physics Communications* 184 (7) (2013) 1701–1707.

- [20] W. Hu, W. Pan, M. Rakhsha, Q. Tian, H. Hu, D. Negrut, A consistent multi-resolution smoothed particle hydrodynamics method, *Computer Methods in Applied Mechanics and Engineering* 324 (2017) 278–299.
- [21] R. Vacondio, B. Rogers, P. Stansby, Accurate particle splitting for smoothed particle hydrodynamics in shallow water with shock capturing, *International Journal for Numerical Methods in Fluids* 69 (8) (2012) 1377–1410.
- [22] R. Vacondio, B. Rogers, P. Stansby, P. Mignosa, Shallow water SPH for flooding with dynamic particle coalescing and splitting, *Advances in Water Resources* 58 (2013) 10–23.
- [23] D. Barcarolo, D. Le Touzé, G. Oger, F. De Vuyst, Adaptive particle refinement and derefinement applied to the smoothed particle hydrodynamics method, *Journal of Computational Physics* 273 (2014) 640–657.
- [24] L. Chiron, G. Oger, M. De Leffe, D. Le Touzé, Analysis and improvements of adaptive particle refinement (APR) through CPU time, accuracy and robustness considerations, *Journal of Computational Physics* 354 (2018) 552–575.
- [25] B. Bouscasse, S. Marrone, A. Colagrossi, A. Di Mascio, Multi-purpose

- interfaces for coupling SPH with other solvers, in: Proceedings of the 8th International SPHERIC Workshop, 2013.
- [26] S. Marrone, A. Di Mascio, D. Le Touzé, Coupling of smoothed particle hydrodynamics with finite volume method for free-surface flows, *Journal of Computational Physics* 310 (2016) 161–180.
- [27] X. Bian, Z. Li, G. Karniadakis, Multi-resolution flow simulations by smoothed particle hydrodynamics via domain decomposition, *Journal of Computational Physics* 297 (2015) 132–155.
- [28] R. Vacondio, B. Rogers, P. Stansby, P. Mignosa, J. Feldman, Variable resolution for SPH: a dynamic particle coalescing and splitting scheme, *Computer Methods in Applied Mechanics and Engineering* 256 (2013) 132–148.
- [29] J. Monaghan, Smoothed particle hydrodynamics, *Rep. Prog. Phys.* vol. 68 (2005) 1–34.
- [30] D. Violeau, *Fluid Mechanics and the SPH Method*, Oxford University Press, 2012.
- [31] L. D. G. Sigalotti, J. Klapp, O. Rendón, C. A. Vargas, F. Peña-Polo, On

- the kernel and particle consistency in smoothed particle hydrodynamics, *Applied Numerical Mathematics* 108 (2016) 242–255.
- [32] G. Vaughan, T. R. Healy, K. R. Bryan, A. D. Sneyd, R. Gorman, Completeness, conservation and error in sph for fluids, *International journal for numerical methods in fluids* 56 (1) (2008) 37–62.
- [33] H. Wendland, Piecewise polynomial, positive definite and compactly supported radial functions of minimal degree, *Advances in computational Mathematics* 4 (1) (1995) 389–396.
- [34] J. P. Morris, P. J. Fox, Y. Zhu, Modeling low reynolds number incompressible flows using sph, *Journal of computational physics* 136 (1) (1997) 214–226.
- [35] D. Molteni, A. Colagrossi, A simple procedure to improve the pressure evaluation in hydrodynamic context using the sph, *Computer Physics Communications* 180 (6) (2009) 861–872.
- [36] M. Antuono, A. Colagrossi, S. Marrone, D. Molteni, Free-surface flows solved by means of SPH schemes with numerical diffusive terms, *Computer Physics Communications* 181 (3) (2010) 532 – 549.

- [37] P. Randles, L. D. Libersky, Smoothed particle hydrodynamics: some recent improvements and applications, *Computer methods in applied mechanics and engineering* 139 (1-4) (1996) 375–408.
- [38] P. Sun, A. Colagrossi, S. Marrone, M. Antuono, A. Zhang, Multi-resolution delta-plus-SPH with tensile instability control: Towards high reynolds number flows, *Computer Physics Communications* 224 (2018) 63–80.
- [39] J. Monaghan, SPH without a tensile instability, *Journal of computational physics* 159 (2) (2000) 290–311.
- [40] T. Krüger, F. Varnik, D. Raabe, Second-order convergence of the deviatoric stress tensor in the standard Bhatnagar-Gross-Krook lattice Boltzmann method, *Phys. Rev. E* 82 (2010) 025701.
- [41] L. Lobovský, E. Botia-Vera, F. Castellana, J. Mas-Soler, A. Souto-Iglesias, Experimental investigation of dynamic pressure loads during dam break, *Journal of Fluids and Structures* 48 (2014) 407 – 434.
- [42] B. Havasi-Tóth, Nauticle: A general-purpose particle-based simulation tool, *Computer Physics Communications* (2019) 106855.